

Linköping University Post Print

Multidimensional Simulations of Magnetic Field Amplification and Electron Acceleration to Near-Energy Equipartition With Ions by a Mildly Relativistic Quasi-Parallel Plasma Collision

GC Murphy, Mark Eric Dieckmann and LOC Drury

N.B.: When citing this work, cite the original article.

©2010 IEEE. Personal use of this material is permitted. However, permission to reprint/republish this material for advertising or promotional purposes or for creating new collective works for resale or redistribution to servers or lists, or to reuse any copyrighted component of this work in other works must be obtained from the IEEE.

GC Murphy, Mark Eric Dieckmann and LOC Drury, Multidimensional Simulations of Magnetic Field Amplification and Electron Acceleration to Near-Energy Equipartition With Ions by a Mildly Relativistic Quasi-Parallel Plasma Collision, 2010, IEEE Transactions on Plasma Science, (38), 10, 2985-2992.

<http://dx.doi.org/10.1109/TPS.2010.2063442>

Postprint available at: Linköping University Electronic Press

<http://urn.kb.se/resolve?urn=urn:nbn:se:liu:diva-60283>

Multidimensional Simulations of Magnetic Field Amplification and Electron Acceleration to Near-Energy Equipartition With Ions by a Mildly Relativistic Quasi-Parallel Plasma Collision

Gareth C. Murphy, Mark E. Dieckmann, and L. O'C. Drury

Abstract—The energetic electromagnetic eruptions observed during the prompt phase of gamma-ray bursts are attributed to synchrotron emissions. The internal shocks moving through the ultrarelativistic jet, which is ejected by an imploding supermassive star, are the likely source of this radiation. Synchrotron emissions at the observed strength require the simultaneous presence of powerful magnetic fields and highly relativistic electrons. We explore with 1-D and 3-D relativistic particle-in-cell simulations the transition layer of a shock, which evolves out of the collision of two plasma clouds at a speed $0.9c$ and in the presence of a quasi-parallel magnetic field. The cloud densities vary by a factor of 10. The number densities of ions and electrons in each cloud, which have the mass ratio 250, are equal. The peak Lorentz factor of the electrons is determined in the 1-D simulation, as well as the orientation and the strength of the magnetic field at the boundary of the two colliding clouds. The relativistic masses of the electrons and ions close to the shock transition layer are comparable as in previous work. The 3-D simulation shows rapid and strong plasma filamentation behind the transient precursor. The magnetic field component orthogonal to the initial field direction is amplified in both simulations to values that exceed those expected from the shock compression by over an order of magnitude. The forming shock is quasi-perpendicular due to this amplification. The simultaneous presence of highly relativistic electrons and strong magnetic fields will give rise to significant synchrotron emissions.

Index Terms—Magnetic confinement, plasma accelerators, plasma simulation, plasma transport processes.

I. INTRODUCTION

MILDLY relativistic plasma collisions are commonly found in astrophysical scenarios, in particularly strong supernovae [1]–[4], in gamma-ray bursts (GRBs) [5]–[8], and in the jets of microquasars [9]–[11] and active galactic nuclei [12]–[14].

Manuscript received December 1, 2009; revised July 12, 2010; accepted July 26, 2010. Date of publication September 9, 2010; date of current version October 8, 2010. This work was supported in part by the Science Foundation Ireland under Grant 08/RFP/PHY1694 and in part by the Swedish Vetenskapsrådet.

G. C. Murphy and L. O'C. Drury are with the Dublin Institute for Advanced Studies, Dublin 2, Ireland (e-mail: gmurphy@cp.dias.ie; ld@cp.dias.ie).

M. E. Dieckmann is with the Department of Science and Technology, Linköping University, 60174 Norrköping, Sweden (e-mail: Mark.E.Dieckmann@itn.liu.se).

Color versions of one or more of the figures in this paper are available online at <http://ieeexplore.ieee.org>.

Digital Object Identifier 10.1109/TPS.2010.2063442

The prompt emissions of the ultrarelativistic GRBs are probably the most spectacular eruptions of electromagnetic radiation in the universe, as they are observed across cosmological distances. Since the first observations of GRBs, thousands have been detected. They all share a common signature of energetic radiation attributed to highly relativistic electrons and strong magnetic fields.

The details of the underlying physical mechanism that causes the prompt emissions are still unknown. In particular, the method by which the magnetic field is generated and sustained, and the means by which electrons are accelerated to ultrarelativistic speeds in sufficient numbers to be injected into the Fermi mechanism, is still under debate. It is therefore interesting and relevant to use numerical simulations to probe the behavior of magnetized shocks to see if a robust mechanism to self-consistently amplify the field may be found.

While the first-order Fermi acceleration mechanism is certainly capable of accelerating particles [15] to ultrarelativistic energies, it requires a seed population of nonthermal particles before it can viably accelerate them to high energies. This mechanism may not also be able to rapidly provide enough for the huge quantities of highly relativistic electrons, which drive the prompt emissions of GRBs. Plasma instabilities driven by the relativistic flow may be a more likely candidate mechanism.

A. Plasma Instabilities

Many instabilities, such as the two-stream, filamentation or Weibel-type, and oblique instabilities, are expected to operate in the relativistic plasma, and it is not a straightforward task to distinguish the dominant mode [16], [17]. The Weibel-type filamentation instability is expected to generate or amplify magnetic fields. Since the pioneering studies of the electromagnetic Weibel instability [18], [19] and of the beam-Weibel or filamentation instability [20]–[22], much work has been done that are both analytical [23]–[26] and numerical using kinetic particle-in-cell (PIC) simulations [27]–[29] and Vlasov simulations [30].

Reconnection in pair plasmas also excites the Weibel instability [31], [32].

Three-dimensional simulations have the best chance to approximate the correct physics; however, they are extremely challenging even for contemporary state-of-the-art supercomputers. It is thus customary to reduce the ion-to-electron mass ratio, to consider only leptonic flows, or to extract aspects of the physically correct 3-D plasma behavior and to model them in 1-D or 2-D grids at the appropriate spatiotemporal resolution. Certain instabilities can be examined in such reduced geometries like the electrostatic two-stream instability in one dimension and the filamentation instability in two dimensions.

B. Previous Related Work on Plasma Collisions and Shock Formation

Early work was done with counterstreaming and interpenetrating electron–positron plasmas, finding filamentation growing [28], [33]. Previous simulation studies of relativistic shocks in more than one spatial dimension have focused on mildly to highly relativistic collision speeds and on symmetric clouds of positron–electron pair plasmas [34]–[37]. These simulations are fast because they only involve one spatiotemporal scale, namely, the leptonic one. However, these scenarios necessarily exclude the wealth of wave modes and nonlinear processes that exist in ion–electron collisions due to the mass asymmetry and the massive kinetic energy of the ions. Relevant PIC simulations are the 3-D simulation with a low mass ratio discussed in [38] and the 2-D simulation with a high mass ratio performed in [39]. Magnetic field effects on the collision of two plasma clouds have also been investigated [40].

In this paper, we consider the simultaneous effects of a high plasma temperature, a quasi-parallel magnetic field, and an initial density asymmetry on the plasma collision. A density asymmetry has been introduced before [38], but here, we increase the density ratio from 3 to 10. This high ratio implies that the initial spectrum of unstable waves should shift from the electromagnetic filamentation instability to the partially electrostatic oblique-mode instability [41]. This shift is further emphasized by the high temperature and the guiding magnetic field, which both reduce the growth rate of the filamentation instability compared with those of the other waves. Section II provides a more detailed overview over the simulation code and the initial conditions. One-dimensional PIC simulations with a similar setup have been first considered in [42]. They have been extended to two dimensions, albeit over a limited spatiotemporal range, in [43]. The 1-D PIC simulation data that we present here in Section III employs a setup that is practically identical to that in [43] apart from the different ion-to-electron mass ratio and code. The simulation results are essentially the same, which is a clear evidence for the actual physical equipartition of the electron and ion energy in the resulting shock. Obtaining this result only for one mass ratio may be a coincidence. The 3-D numerical simulation also presented in Section III extends the 2-D simulation in [43], confirming that the front of the dense cloud is practically planar. The 1-D PIC simulation is thus, at least initially, a good approximation for the plasma dynamics close to the front of the expanding dense cloud. However, the plasma density distribution clearly

evidences filamentation behind this front, which is not revealed to this extent by the electromagnetic fields in [43].

II. INITIAL CONDITIONS AND NUMERICAL METHOD

Two plasma clouds collide in the simulation box. The species 1 and 2 are the electrons and ions of the dense cloud, whereas the electrons and ions of the tenuous cloud are the species 3 and 4, respectively. The species number gives the subscript j of the density n_j . Each cloud has electrons and ions with the mass ratio $R = m_i/m_e = 250$, with the same density ($n_1 = n_2$ and $n_3 = n_4$), temperature, and mean speed. Each cloud is thus initially charge and current neutral. The mean velocity vectors of both clouds point along opposite x -directions, and they have the same modulus v_b . Each cloud initially occupies one half of the simulation box, and their contact boundary is located at $x = 0$ at the time $t = 0$. Both clouds are uniform along the y - and z -directions. No particles are introduced at the boundaries for $t > 0$. The clouds, thus, instantly detach from the walls, and we can use periodic boundary conditions in all directions. A guiding magnetic field \mathbf{B}_0 gives an electron gyrofrequency $\omega_c = e|\mathbf{B}_0|/m_e$ that is equal to the electron plasma frequency $\omega_{p1} = (e^2 n_1/m_e \epsilon_0)^{1/2}$ of the dense cloud. \mathbf{B}_0 is quasi-parallel to the flow (x) direction, and at $t = 0$, $B_{0,x} \gg B_{0,z}$ and $B_{0,y} = 0$. The convection electric field $E_c = |v_b B_{0,z}|$ changes its sign across the collision boundary. The collision speed $2v_b/(1 + v_b^2/c^2) = 0.9c$, and the electron thermal velocity $v_t = (T_e/m_e)^{1/2}$ for $T_e = 131$ keV is $\approx c/2$. We express space and time in the relevant units of the dense ions (species 2), which are the ion skin depth $\lambda_2 = c/\omega_{p2}$ with $\omega_{p1}^2/\omega_{p2}^2 = R$ and the inverse ion plasma frequency ω_{p2}^{-1} .

We use the PIC method described in detail in [44]. The normalized equations are

$$\nabla \times \mathbf{E} = -\frac{\partial \mathbf{B}}{\partial t} \quad (1)$$

$$\nabla \times \mathbf{B} = \frac{\partial \mathbf{E}}{\partial t} + \mathbf{J} \quad (2)$$

$$\nabla \cdot \mathbf{B} = 0 \quad (3)$$

$$\nabla \cdot \mathbf{E} = \rho \quad (4)$$

$$\frac{d\mathbf{p}_j}{dt} = q_i(\mathbf{E} + \mathbf{v}_j \times \mathbf{B}) \quad (5)$$

$$\mathbf{p}_j = m_k \Gamma_j \mathbf{v}_j \quad (6)$$

$$\frac{d\mathbf{x}_j}{dt} = \mathbf{v}_j. \quad (7)$$

The particle j of species k has the mass m_k . The quantities in SI units (subscript p) can be obtained by the substitutions $\mathbf{E}_p = \omega_{p2} c m_i \mathbf{E}/e$, $\mathbf{B}_p = \omega_{p2} m_i \mathbf{B}/e$, $\rho_p = en_2 \rho$, $\mathbf{J}_p = ec n_2 \mathbf{J}$, $\mathbf{x}_p = \lambda_2 \mathbf{x}$, and $t_p = t/\omega_{p2}$.

The simulation resolution is as follows: For the 1-D simulation, we use 18 000 cells along x and 250 particles per cell. For the 3-D simulation, we can only simulate a small fraction of the 1-D domain with regard to x , but we get instead a view of the early 3-D filament formation. We use 20 particles per cell and a 3-D box composed of

TABLE I
PHYSICAL PARAMETERS

Parameter	Value
Thermal Velocity	$0.52c$
Collision Speed	$0.9c$
Beam Speed	$0.63c$
Temperature	131 keV
Mass ratio	250
Field Angle	0.1 radians
Density Ratio	10

TABLE II
NUMERICAL PARAMETERS

Parameter	1D	3D
No. particles/cell	250	20
No. Cells	18000	$1500x100x100$
Timestep	$8.6e-2 \omega_{p1}^{-1}$	$8.6e-2 \omega_{p1}^{-1}$

$1500 \times 100 \times 100$ cells, which spans a total of $15\lambda_2 \times 1.25\lambda_2 \times 1.25\lambda_2$ and a long direction aligned with x . The timesteps for the 1-D and 3-D simulations are both $8.6e2\omega_{p1}^{-1}$. The physical and simulation parameters are summarized in Tables I and II, respectively.

III. RESULTS

A. 1-D Simulation

A circularly polarized electromagnetic wave grows practically instantly at the contact boundary of both clouds and in both simulations. This collision boundary evolves due to the plasma counterstream into a cloud overlap layer. The magnetic field is frozen in into each cloud outside the overlap layer. Inside this layer, the magnetic field continues to be practically at rest in the reference frame of the dense plasma cloud. The tenuous cloud moves at a mildly relativistic speed relative to this reference frame, and the particles are deflected by \mathbf{B}_0 . The ions and electrons differently react to \mathbf{B}_0 , and due to its obliqueness, the particles are forced onto an orbit that involves all components of \mathbf{p} . This corkscrew orbit is discussed in more detail elsewhere [43]. The resulting net current amplifies the magnetic field perturbation, and a circularly polarized localized wave structure forms.

Fig. 1 displays the most relevant phase-space distributions. These are the electron distribution $f_e(\Gamma, x)$ and the ion distribution $f_i(x, p_x)$. The electron distribution reveals the peak energies reached by the electrons, whereas the ion distribution can reveal the formation of a shock. This is achieved when the ion distributions of both clouds mix in this phase-space projection. The 1-D simulation stops at the time $t = 84$, just before the shock formation. The electron distribution demonstrates that the electrons of the tenuous cloud (species 3) are forced onto a strong oscillation, which resembles a corkscrew orbit by the rotation in the $p_y p_z$ plane. They reach a peak $\Gamma \approx 50$ at $x \approx 43$. The electrons of the dense cloud (species 1), on the other hand, are not yet accelerated on this scale. The electrons of both clouds show a two-stream configuration in the interval $30 < x < 43$. The electrons would drive

the oblique-mode instability, which is here suppressed by the 1-D geometry. Only the electrostatic two-stream instability can develop here, and it results in the thermalization of the electrons of the tenuous cloud. This thermalization results in the hot electron population with $x < 30$ and with $\Gamma \leq 25$. The phase speed of the two-stream waves is close to the beam speed of the tenuous beam, and only those resonantly interact with this wave. The electron phase-space distribution of the dense cloud thus remains practically unchanged. The ion phase-space distribution reveals that a shock is about to form at $x \approx 40$. The circularly polarized energetic electromagnetic structure (EES) is here strong enough to force the ions onto a corkscrew orbit. In particular, the ions of the tenuous cloud (species 4) are perturbed within the cloud overlap layer. The beam striation in the $x p_x$ plane implies that the associated fields must be at least partially electrostatic. Electrostatic fields and such phase-space striation are reminiscent of the Buneman instability, which would develop here between the ions of the tenuous cloud and the electrons of the dense one [45].

Fig. 2 displays the distributions of all components of \mathbf{B} and \mathbf{E} near the front of the dense cloud at the time $t = 84$, which corresponds to the particle distribution in Fig. 1. The upper panel shows that all components of \mathbf{E} have reached a comparable strength. The electromagnetic E_y and E_z are phase shifted by 90° . The magnetic B_y and B_z components (lower panel) also show this phase shift. We find that $B_x = B_{x,0}$. B_x must remain constant in a 1-D simulation by $\nabla \cdot \mathbf{B} = 0$, and a change of B_x in time could only be driven by $\partial_y E_z - \partial_z E_y \neq 0$, which is not possible in 1-D. The asymmetry in space of the EES that is relative to its amplitude maximum may reflect the varying plasma skin depth across the collision boundary. The skin depth is reduced by a factor $\sqrt{10}$ in the dense plasma. If the penetration depth of the EES is a few ion skin depths, then the wave envelope must decrease more quickly as it enters the dense plasma.

The electrostatic component E_x is strong in the interval where the electromagnetic fields (E_y and E_z) are strong. The electromagnetic fields are tied to the circularly polarized wave structure, which provides the dissipation of the flow energy. E_x is such that electrons are accelerated to the left within $42 < x < 47$. This electric field must develop between the ions and the electrons of the tenuous cloud because the dense cloud in Fig. 1 has not propagated yet that far. The likely cause is the deflection of the electrons of species 3 by the EES. A mere rotation of the electron velocity vector away from the x -direction would decrease their flow velocity along x . The ion speed remains practically unaffected, and an electric charge builds up. The charge results in an electrostatic field, which drags the electrons with the ions. The electrons are accelerated at the expense of the ion kinetic energy. This explains the decrease in the flow speed modulus of the ions of the tenuous cloud and the electron acceleration in this interval.

The EES at the front of the dense cloud has a wave vector parallel to x , and it can thus be resolved by the 1-D simulation. The electromagnetic instabilities in the cloud overlap layer, e.g., the filamentation and oblique-mode instabilities, cannot develop here because their wave vectors are orthogonal or oblique to the beam velocity vector. The plasma dynamics in the cloud overlap layer, thus, cannot be accurately resolved by the

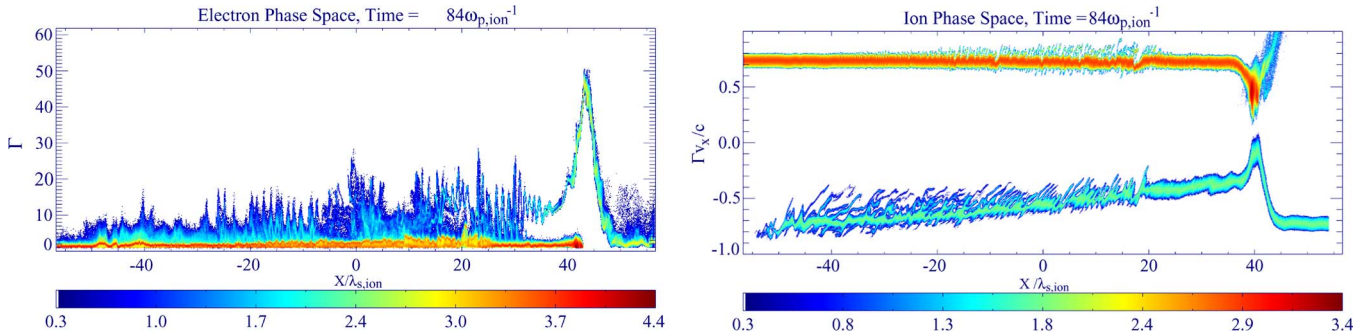


Fig. 1. (Left) Electron phase-space density $f_e(\Gamma, x)$. (Right) Ion phase-space density $f_i(\Gamma v_x/c, x)$. The color scale is 10-logarithmic, and the density is expressed in units of a computational particle of the tenuous cloud.

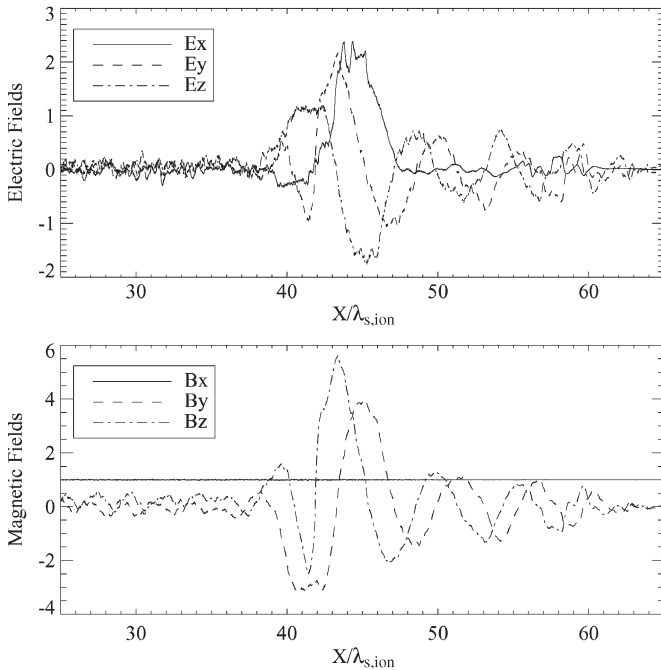


Fig. 2. EES in 1-D: plots of electric and magnetic field strengths. (Upper panel) Components of \mathbf{E} . (Lower panel) Components of \mathbf{B} .

1-D simulation, which overemphasizes the importance of the electrostatic two-stream and Buneman instabilities with their flow-aligned wave vectors. We turn to the 3-D simulation, with which we can resolve the full-wave spectrum during the first few inverse ion plasma frequencies.

B. 3-D Plasma Filament Structure

The 3-D simulation is initialized in the same manner as the 1-D simulation, except over a smaller domain along x , due to computational constraints. Consequently, the simulation is run over the significantly shorter time interval $t = 6$ than the 1-D simulation with its $t = 84$. This time is also somewhat shorter than the run time of the 2-D PIC simulation in [43], which ran for about 11 inverse ion plasma frequencies for the mass ratio 400. This previous work examined the electromagnetic wave structures, particularly at the front of the dense cloud and the simulation’s end, showing that they have remained planar. Here, we do not look at the field topology but at the ion density distribution in the entire simulation box.

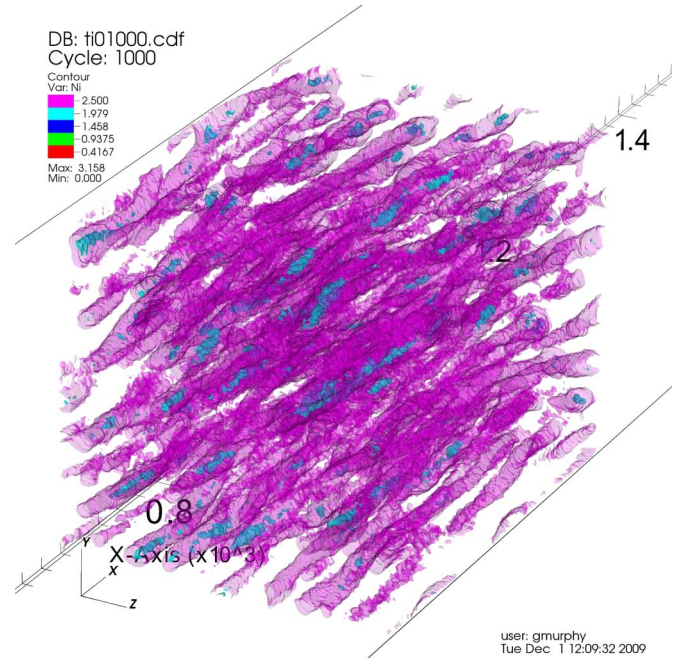


Fig. 3. Three-dimensional rendering of a simulation of plasma collision. Two isosurfaces of logarithm of ion density are shown at values of 2.5 and 1.9. The filaments are preferentially aligned along the x -axis, gyrating in the yz plane.

Fig. 3 shows the 3-D rendering of the ion density in our numerical simulation. Clearly, the counterstreaming ions in three dimensions quickly form filaments, which result in an amplification of the magnetic field orthogonal to the filament axis. These magnetic fields grow until they saturate through magnetic trapping [20]. The strength B_0 of the guiding magnetic field has been selected to suppress the filamentation and oblique-mode instabilities driven by the electrons [46] in a spatially uniform two-beam configuration. The magnetic field strength has been apparently insufficient to suppress the filamentation and mixed-mode instabilities in the presence of ions and of a spatial nonuniformity. A further increase in the amplitude of B_0 would be necessary to achieve this [40], but such a field is probably unrealistic for most astrophysical plasmas. The filaments have a preferential alignment with the initial flow velocity vector. This is not surprising because the filamentation and oblique-mode instabilities yield the growth of a magnetic field through the redistribution of the microcurrents carried by the moving charged particles. These microcurrents $\propto q\mathbf{v}$ are obviously strongest along the mean flow (x) direction.

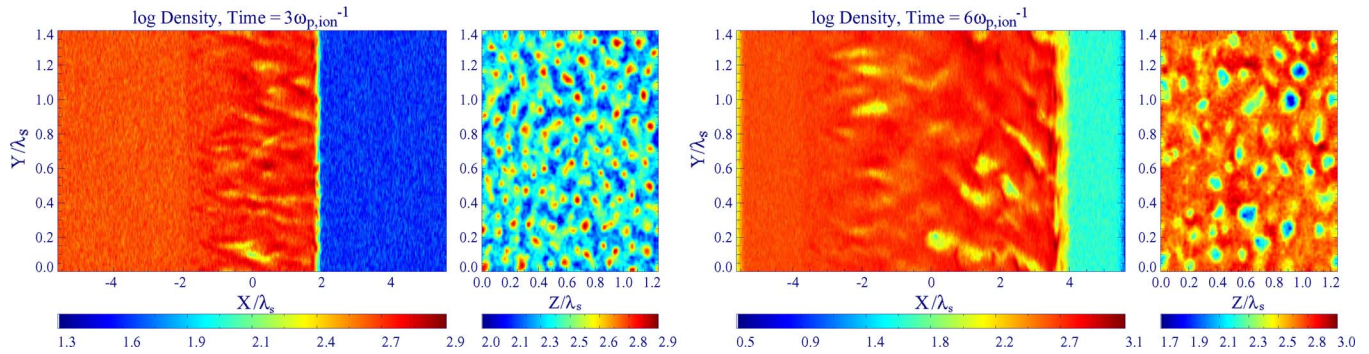


Fig. 4. Growth and merging of filaments in 3-D: ion density plots at times $t = 3$ and $t = 6$. Filaments, which are characterized through density modulations, have increased in size.

This preferential alignment of the filaments with the x -direction allows us to obtain insight into the filament thickness with slices in the yz plane. Their coherence length along the filament axis can be estimated from 2-D cross sections in the xy plane. In Fig. 4, we plot these 2-D cuts from the 3-D simulation at the times $t = 3$ and $t = 6$. We clearly see the formation of filaments in the ion density distribution, which we identify through a density modulation. Their characteristic diameter is well below 0.1 ion inertial length at $t = 3$ and is thus comparable with the electron skin depth of the dense cloud $\lambda_1 = \lambda_2/\sqrt{R}$. The filament diameter increases beyond 0.1 ion inertial length through the dynamical interaction and the mergers of filaments [47]. This small size suggests that, until $t = 6$, the main driver of the ion beam filamentation has been the electrons. The cut of the ion distribution in the yz plane in the right panel of Fig. 4 shows some filaments with a significant density depletion and with a radial cross section. Examples are the low-density structures at $z \approx 1.0$ and $0.9 < y < 1.2$. These are ion filaments immersed in an almost spatially uniform ion background. The ion density is reduced, and the small spatial scale suggests that the ions merely follow the electron density to maintain the quasi-neutrality of the plasma. The electron density can be decreased through a magnetic expulsion of the electrons of one of the clouds. The coherence length in the xy plane is about an ion skin depth, which is an order of magnitude larger than the filament diameter. Some of these filaments may thus be described well by their cross section in the yz plane, which neglects changes along x . We furthermore find that the spatial separation of these radial filaments is larger than their diameter, which implies that these filaments may not magnetically interact over a limited time interval. Equilibrium might be possible during this time between the filament and the spatially uniform background plasma. This equilibrium may be similar to the Hammer–Rostoker equilibrium for a tenuous relativistic electron beam that crosses a dense electron background [48]. The agreement is not exact. Here, the ions react to the electric charge built up by the expulsion of the background electrons from the flux tube, and the plasma carries an oblique magnetic field. Both aspects have not been considered in [48].

Finally, we notice from the right panel in Fig. 4 that the filamentation also involves the front of the dense cloud at $x \approx 4$. This filamentation is fairly weak, and its scale is again a fraction of the ion skin depth. This implies that a 1-D simulation cannot

reproduce the exact physics at the cloud front, but at least until $t = 6$, this approximation is fairly accurate. It is interesting that filamentation was not observed in the 2-D simulation in [43] that covered a longer time interval. Several reasons are possible. First, the higher ion mass in the 2-D simulation may have delayed the ion filamentation in the yz plane with respect to the formation of the EES, which modulates the ions along x . Both are competing processes. Second, the field distribution was used in [43] to determine the planarity of the cloud front, whereas the ion density is considered here. The magnetic field amplification by the filamentation instability is much weaker than that by the EES, and it may not be visible. The ion density modulation along yz can thus more accurately reveal the filamentation than the electromagnetic fields. The electromagnetic fields due to the EES reach a much higher energy density than those due to the filamentation instability also in the 3-D simulation, which we now show.

C. EES in 3-D

The EES acts to accelerate charged particles; it can provide the energy dissipation that enforces the formation of a shock, and it may provide a compact location for synchrotron radiation in the shock transition layer. The size scale and the energy density is similar to that detected in the short large-amplitude magnetized structures, which have been observed both in simulations and in those regions of the Earth’s bow shock, where the ambient magnetic field is quasi-parallel to the shock normal [43], [49]–[52].

In Fig. 5, we see for the first time in 3-D the EES. We make use of the quasi-planarity of the front of the dense cloud at $t = 3$ in Fig. 4, and we integrate the energy densities of the electromagnetic fields along y and z , which reduces the noise levels. The energy densities naturally subdivide into 1) B_x^2 , which is unchanged in a 1-D simulation; into 2) $B_{\text{perp}}^2 = B_y^2 + B_z^2$ and 3) $E_{\text{perp}}^2 = E_y^2 + E_z^2$, which would be purely electromagnetic in a 1-D simulation; and into 4) E_x^2 , which would be electrostatic. This distinction is strictly possible only in 1-D because the derivatives along y and z vanish in the Maxwell’s equations. We expect that, initially and due to the planarity of the wave structures, this also holds in 3-D. All energy densities are normalized to the same value, which is the energy density of \mathbf{B}_0 .

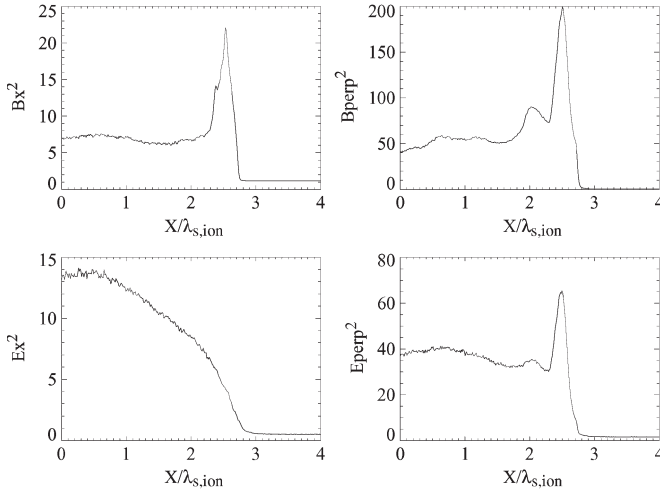


Fig. 5. Electromagnetic energy densities at $t = 3$. (Left panels) Energy densities B_{\perp}^2 and E_{\perp}^2 along the initial flow velocity vector. (Right panels) $B_{\text{perp}}^2 = B_y^2 + B_z^2$ and $E_{\text{perp}}^2 = E_y^2 + E_z^2$ orthogonal to the initial flow direction.

Already at this early simulation time, all energy densities surpass by far the initial magnetic energy density as the front of the dense plasma cloud is crossed from the upstream into the cloud overlap layer. The dominant component is B_{perp} , as in the 1-D simulation. It peaks at $x \approx 2.6$, which is ahead of the dense cloud. The peak of E_{perp} coincides with this location, and both thus belong to the same wave structure. Note that even if the EES were purely magnetic in its rest frame, the convective electric field would be significant due to its rapid propagation. The 3-D simulation facilitates the growth of B_x^2 and its peak energy density, which is an order of magnitude less than that of B_{perp}^2 , is reached at the same position $x = 2.6$ as that of B_{perp}^2 . E_x^2 in the 3-D simulation shows like that of B_x^2 , a distribution that strongly differs from its equivalent in the 1-D simulation. It steadily grows as we go from $x = 3$ to $x = 0.5$. The electric field in the 1-D simulation peaked where the EES was strongest. We interpret the changed distribution E_x^2 in the following way. Let us assume that the E_x is entirely driven in 1-D by the different deflection of the electrons and the ions of the tenuous cloud. The quasi-neutrality of the plasma of the tenuous cloud can then only be maintained by a flow along x , whereas a 3-D simulation also enables a flow of charges along y and z . This will, in turn, alter the electric field distribution. The apparent consequence is that E_x^2 disappears within the EES. We may attribute instead the increase in E_x^2 in the 3-D simulation to the particle heating. The energy density of the electrostatic fluctuations is proportional to the plasma temperature if the plasma is in equilibrium (see [53] and references therein). Evidence for this connection is that $E_{\text{perp}}^2 \approx 2E_x^2$, and the energy density per degree of freedom is thus similar. Since the electrostatic energy density in thermal equilibrium is also proportional to the particle mass, it is exaggerated by the low statistical plasma representation by a PIC code. The energy density of the EES is, on the other hand, independent of the mass of a computational particle and determined by the kinetic energy density of the inflowing plasma. We may expect that, in reality, the electromagnetic energy would far exceed the electrostatic one.

IV. CONCLUSION

In this paper, we have presented the results of the long term 1-D and the short-term 3-D simulations of plasma collisions. We found that, in 1-D, a strong amplification of the field is found in the foreshock, in excess of that expected from compression alone. Strong circularly polarized electromagnetic waves are generated at the collision boundary. We find that electrons are accelerated to ultrarelativistic speeds and that the presence of the EES is confirmed in 3-D. The quasi-parallel magnetic field fails to suppress the filamentation in three dimensions, which was not detected in 2-D fields in previous work, probably obscured in the data due to the large contrast provided by the EES. Ion densities are found to be a much better indicator for current filaments. The 3-D structure of the EES differs from its 1-D model; in particular, the parallel electric field is diminished at the collision boundary and is only excited by electron heating. Filaments are produced with a characteristic width of approximately 0.1 ion inertial length and a larger separation between filaments, indicating a possibility for magnetized Hammer–Rostoker equilibrium. The presence and size of the EES could be critical for the acceleration of matter to high energies in plasma shocks. The simulations show the relevance of 3-D simulations, even over small physical scales.

The EES is relevant to the problem of the large fields and electron acceleration needed to explain the observations of spectra of GRBs. The study shows that the EES is stable in 3-D and that the magnetic field is amplified in 3-D. Comparing other magnetic field amplification mechanisms such as Bell's instability [55], this mechanism does not require addition of external current but produces electron acceleration to near-equipartition speeds and a strongly self-consistently amplified field. Shock compression can also amplify the field but only up to a factor f , $4 < f < 7$, depending on the value of the ratio of specific heats. In this respect, it is an important result.

For future work, we need significantly longer timescales to confirm the long-term stability of EES. Two-dimensional simulations are already under way with the goal of estimating the long-term evolution of the system at high resolution.

ACKNOWLEDGMENT

The authors would like to thank the Science Foundation Ireland/Higher Education Authority, Irish Centre for High-End Computing, for providing computational facilities and support. The Plasma Simulation Code was developed by H. Ruhl at Ruhr University Bochum.

REFERENCES

- [1] K. Koyama, R. Petre, E. V. Gotthelf, U. Hwang, M. Matsuura, M. Ozaki, and S. S. Holt, "Evidence for shock acceleration of high-energy electrons in the supernova remnant SN1006," *Nature*, vol. 378, pp. 255–258, Nov. 1995.
- [2] S. R. Kulkarni, D. A. Frail, M. H. Wieringa, R. D. Ekers, E. M. Sadler, R. M. Wark, J. L. Higdon, E. S. Phinney, and J. S. Bloom, "Radio emission from the unusual supernova 1998bw and its association with the γ -ray burst of 25 April 1998," *Nature*, vol. 395, no. 6703, pp. 663–669, Oct. 1998.
- [3] R. Enomoto, T. Tanimori, T. Naito, T. Yoshida, S. Yanagita, M. Mori, P. G. Edwards, A. Asahara, G. V. Bicknell, S. Gunji, S. Hara, T. Hara, S. Hayashi, C. Itoh, S. Kabuki, F. Kajino, H. Katagiri, J. Kataoka,

- A. Kawachi, T. Kifune, H. Kubo, J. Kushida, S. Maeda, A. Maeshiro, Y. Matsubara, Y. Mizumoto, M. Moriya, H. Muraishi, Y. Muraki, T. Nakase, K. Nishijima, M. Ohishi, K. Okumura, J. R. Patterson, K. Sakurazawa, R. Suzuki, D. L. Swaby, K. Takano, T. Takano, F. Tokanai, K. Tsuchiya, H. Tsunoo, K. Uruma, A. Watanabe, and T. Yoshikoshi, "The acceleration of cosmic-ray protons in the supernova remnant RX J1713.7-3946," *Nature*, vol. 416, no. 6883, pp. 823–826, Apr. 2002.
- [4] A. Bamba, R. Yamazaki, M. Ueno, and K. Koyama, "Small-scale structure of the SN 1006 shock with Chandra observations," *Astrophys. J.*, vol. 589, pp. 827–837, Jun. 2003.
- [5] T. Piran, "Gamma-ray bursts and the fireball model," *Phys. Rep.*, vol. 314, pp. 575–667, Jun. 1999.
- [6] M. V. Medvedev and A. Loeb, "Generation of magnetic fields in the relativistic shock of gamma-ray burst sources," *Astrophys. J.*, vol. 526, no. 2, pp. 697–706, Dec. 1999.
- [7] M. Lyutikov and R. Blandford, "Gamma ray bursts as electromagnetic outflows," astro-ph/0312347, Dec. 2003.
- [8] D. B. Fox and P. Mészáros, "GRB fireball physics: Prompt and early emission," *New J. Phys.*, vol. 8, no. 9, p. 199, Sep. 2006.
- [9] R. P. Fender, S. T. Garrington, D. J. McKay, T. W. B. Muxlow, G. G. Pooley, R. E. Spencer, A. M. Stirling, and E. B. Waltman, "MERLIN observations of relativistic ejections from GRS 1915+105," *Mon. Not. Roy. Astron. Soc.*, vol. 304, no. 4, pp. 865–876, Apr. 1999.
- [10] C. R. Kaiser, R. Sunyaev, and H. C. Spruit, "Internal shock model for microquasars," *Astron. Astrophys.*, vol. 356, pp. 975–988, Apr. 2000.
- [11] O. Jamil, R. P. Fender, and C. R. Kaiser, "iShocks: X-ray binary jets with an internal shocks model," *Mon. Not. Roy. Astron. Soc.*, vol. 401, no. 1, pp. 394–404, Jan. 2010.
- [12] M. J. Rees, "The M87 jet—Internal shocks in a plasma beam," *Mon. Not. Roy. Astron. Soc.*, vol. 184, pp. 61P–65P, Sep. 1978.
- [13] M. Spada, G. Ghisellini, D. Lazzati, and A. Celotti, "Internal shocks in the jets of radio-loud quasars," *Mon. Not. Roy. Astron. Soc.*, vol. 325, no. 4, pp. 1559–1570, Aug. 2001.
- [14] S. Sahayanathan and R. Misra, "Interpretation of the radio/X-ray knots of AGN jets within the internal shock model framework," *Astrophys. J.*, vol. 628, no. 2, pp. 611–616, Aug. 2005.
- [15] L. O. Drury, "An introduction to the theory of diffusive shock acceleration of energetic particles in tenuous plasmas," *Rep. Prog. Phys.*, vol. 46, pp. 973–1027, Aug. 1983.
- [16] A. Bret, "Weibel, two-stream, filamentation, oblique, Bell, Buneman . . . Which one grows faster?" *Astrophys. J.*, vol. 699, no. 2, pp. 990–1003, Jul. 2009.
- [17] M. Lemoine and G. Pelletier, "On electromagnetic instabilities at ultra-relativistic shock waves," *Mon. Not. Roy. Astron. Soc.*, vol. 402, no. 1, p. 1732, Nov. 2009.
- [18] E. S. Weibel, "Spontaneously growing transverse waves in a plasma due to an anisotropic velocity distribution," *Phys. Rev. Lett.*, vol. 2, no. 3, pp. 83–84, Feb. 1959.
- [19] R. L. Morse and C. W. Nielson, "Numerical simulation of the Weibel instability in one and two dimensions," *Phys. Fluids*, vol. 14, no. 4, pp. 830–840, Apr. 1971.
- [20] R. C. Davidson, D. A. Hammer, I. Haber, and C. E. Wagner, "Nonlinear development of electromagnetic instabilities in anisotropic plasmas," *Phys. Fluids*, vol. 15, no. 2, pp. 317–333, Feb. 1972.
- [21] R. Lee and M. Lampe, "Electromagnetic instabilities, filamentation, and focusing of relativistic electron beams," *Phys. Rev. Lett.*, vol. 31, no. 23, pp. 1390–1393, Dec. 1973.
- [22] K. Molvig, "Filamentary instability of a relativistic electron beam," *Phys. Rev. Lett.*, vol. 35, no. 22, pp. 1504–1507, 1975.
- [23] R. Z. Sagdeev, "The 1976 Oppenheimer lectures: Critical problems in plasma astrophysics. II. Singular layers and reconnection," *Rev. Mod. Phys.*, vol. 51, no. 1, pp. 11–20, Jan. 1979.
- [24] A. Bret, M.-C. Firpo, and C. Deutsch, "Collective electromagnetic modes for beam–plasma interaction in the whole k space," *Phys. Rev. E, Stat. Phys. Plasmas Fluids Relat. Interdiscip. Top.*, vol. 70, no. 4, p. 046401, Oct. 2004.
- [25] A. Bret, M.-C. Firpo, and C. Deutsch, "Characterization of the initial filamentation of a relativistic electron beam passing through a plasma," *Phys. Rev. Lett.*, vol. 94, no. 11, p. 115002, Mar. 2005.
- [26] M. Lazar, A. Smolyakov, R. Schlickeiser, and P. K. Shukla, "A comparative study of the filamentation and Weibel instabilities and their cumulative effect. I. Non-relativistic theory," *J. Plasma Phys.*, vol. 75, no. 1, p. 19, 2009.
- [27] M. Honda, J. Meyer-ter-Vehn, and A. Pukhov, "Two-dimensional particle-in-cell simulation for magnetized transport of ultra-high relativistic currents in plasma," *Phys. Plasmas*, vol. 7, no. 4, pp. 1302–1308, Apr. 2000.
- [28] L. O. Silva, R. A. Fonseca, J. W. Tonge, W. B. Mori, and J. M. Dawson, "On the role of the purely transverse Weibel instability in fast ignitor scenarios," *Phys. Plasmas*, vol. 9, no. 6, pp. 2458–2461, Jun. 2002.
- [29] A. Stockem, M. E. Dieckmann, and R. Schlickeiser, "Suppression of the filamentation instability by a flow-aligned magnetic field: Testing the analytic threshold with PIC simulations," *Plasma Phys. Control. Fusion*, vol. 50, no. 2, p. 025002, Feb. 2008.
- [30] F. Califano, T. Cecchi, and C. Chiuderi, "Nonlinear kinetic regime of the Weibel instability in an electron–ion plasma," *Phys. Plasmas*, vol. 9, no. 2, pp. 451–457, Feb. 2002.
- [31] S. Zenitani and M. Hesse, "The role of the Weibel instability at the reconnection jet front in relativistic pair plasma reconnection," *Phys. Plasmas*, vol. 15, no. 2, p. 022101, Feb. 2008.
- [32] M. Swisdak, Y. Liu, and J. F. Drake, "Development of a turbulent outflow during electron–positron magnetic reconnection," *Astrophys. J.*, vol. 680, no. 2, pp. 999–1008, Jun. 2008.
- [33] L. O. Silva, R. A. Fonseca, J. W. Tonge, J. M. Dawson, W. B. Mori, and M. V. Medvedev, "Interpenetrating plasma shells: Near-equipartition magnetic field generation and nonthermal particle acceleration," *Astrophys. J.*, vol. 596, no. 1, pp. L121–L124, Oct. 2003.
- [34] Y. Kazimura, J. I. Sakai, T. Neubert, and S. V. Bulanov, "Generation of a small-scale quasi-static magnetic field and fast particles during the collision of electron–positron plasma clouds," *Astrophys. J.*, vol. 498, no. 2, pp. L183–L186, Apr. 1998.
- [35] A. Spitkovsky, "Simulations of relativistic collisionless shocks: Shock structure and particle acceleration," in *Astrophysical Sources of High Energy Particles and Radiation*, T. Bulik, B. Rudak, and G. Madejski, Eds. College Park, MD: AIP, Nov. 2005, ser. American Institute of Physics Conference Series, pp. 345–350.
- [36] L. Sironi and A. Spitkovsky, "Particle acceleration in relativistic magnetized collisionless pair shocks: Dependence of shock acceleration on magnetic obliquity," *Astrophys. J.*, vol. 698, no. 2, pp. 1523–1549, Jun. 2009.
- [37] K. I. Nishikawa, J. Niemiec, P. E. Hardee, M. Medvedev, H. Sol, Y. Mizuno, B. Zhang, M. Pohl, M. Oka, and D. H. Hartmann, "Weibel instability and associated strong fields in a fully three-dimensional simulation of a relativistic shock," *Astrophys. J. Lett.*, vol. 698, no. 1, pp. L10–L13, May 2009.
- [38] J. T. Frederiksen, C. B. Hededal, T. Haugbølle, and Å. Nordlund, "Magnetic field generation in collisionless shocks: Pattern growth and transport," *Astrophys. J.*, vol. 608, no. 1, pp. L13–L16, Jun. 2004.
- [39] A. Spitkovsky, "On the structure of relativistic collisionless shocks in electron–ion plasma plasmas," *Astrophys. J. Lett.*, vol. 673, no. 1, pp. L39–L42, Dec. 2008.
- [40] C. B. Hededal and K.-I. Nishikawa, "The influence of an ambient magnetic field on relativistic collisionless plasma shocks," *Astrophys. J.*, vol. 623, no. 2, pp. L89–L92, Apr. 2005.
- [41] A. Bret, L. Gremillet, and J. Bellido, "How really transverse is the filamentation instability?" *Phys. Plasmas*, vol. 14, no. 3, p. 032103, Mar. 2007.
- [42] N. Bessho and Y. Ohsawa, "Electron acceleration to ultrarelativistic energies in a collisionless oblique shock wave," *Phys. Plasmas*, vol. 6, no. 8, pp. 3076–3085, Aug. 1999.
- [43] M. E. Dieckmann, P. K. Shukla, and L. O. C. Drury, "The formation of a relativistic partially electromagnetic planar plasma shock," *Astrophys. J.*, vol. 675, no. 1, pp. 586–595, Mar. 2008.
- [44] J. M. Dawson, "Particle simulation of plasmas," *Rev. Mod. Phys.*, vol. 55, no. 2, pp. 403–447, Apr. 1983.
- [45] O. Buneman, "Instability, turbulence, and conductivity in current-carrying plasma," *Phys. Rev. Lett.*, vol. 1, no. 1, pp. 8–9, Jul. 1958.
- [46] A. Bret, M. E. Dieckmann, and C. Deutsch, "Oblique electromagnetic instabilities for a hot relativistic beam interacting with a hot and magnetized plasma," *Phys. Plasmas*, vol. 13, no. 8, p. 082109, Aug. 2006.
- [47] T. J. Bogdan and I. Lerche, "Dynamical evolution of large-scale two-dimensional, fibril magnetic fields," *Astrophys. J.*, vol. 296, pp. 719–738, Sep. 1985.
- [48] D. A. Hammer and N. Rostocker, "Propagation of high current relativistic electron beams," *Phys. Fluids*, vol. 13, no. 7, pp. 1831–1850, 1970.
- [49] G. Mann, H. Luhr, and W. Baumjohann, "Statistical analysis of short large-amplitude magnetic field structures in the vicinity of the quasi-parallel bow shock," *J. Geophys. Res.*, vol. 99, no. A7, pp. 13 315–13 323, Jan. 1994.
- [50] R. Behlke, M. Andre, S. C. Buchert, A. Vaivads, A. I. Eriksson, E. A. Lucek, and A. Balogh, "Multi-point electric field measurements of short large-amplitude magnetic structures (slams) at the earth's quasi-parallel bow shock," *Geophys. Res. Lett.*, vol. 30, p. 1177, Feb. 2003.

- [51] K. Tsubouchi and B. Lembege, "Full particle simulations of short large-amplitude magnetic structures (slams) in quasi-parallel shocks," *J. Geophys. Res.*, vol. 109, no. A2, p. A02114, Feb. 2004.
- [52] M. E. Dieckmann, G. C. Murphy, A. Meli, and L. O. C. Drury, "Particle-in-cell simulation of a mildly relativistic collision of an electron-ion plasma carrying a quasi-parallel magnetic field. Electron acceleration and magnetic field amplification at supernova shocks," *Astron. Astrophys.*, vol. 509, p. A89, Jan. 2010.
- [53] M. E. Dieckmann, A. Ynnerman, S. C. Chapman, G. Rowlands, and N. Andersson, "Simulating thermal noise," *Phys. Scr.*, vol. 69, no. 6, pp. 456–460, 2004.
- [54] V. L. Krasovsky, "Trapped particle effect on the velocity of circularly polarized electromagnetic waves in an isotropic plasma," *Phys. Lett. A*, vol. 374, no. 15/16, pp. 1751–1754, Apr. 2010.
- [55] A. R. Bell, "Turbulent amplification of magnetic field and diffusive shock acceleration of cosmic rays," *Mon. Not. Roy. Astron. Soc.*, vol. 353, no. 2, pp. 550–558, Sep. 2004.



Gareth C. Murphy received the B.E. degree in electronic engineering from the University College Dublin, Dublin, Ireland, in 2002 and the Ph.D. degree for the study of 3-D magnetohydrodynamical jets from Trinity College Dublin, Dublin, in 2007.

He held a postdoctoral fellowship with the Laboratoire d'Astrophysique de Grenoble, Grenoble, France, from 2006 to 2009. He is currently holding a Science Foundation Ireland postdoctoral fellowship with the Dublin Institute for Advanced Studies, Dublin. His research interests include shock waves,

astrophysical plasma dynamics, laser-plasma interaction, and massively parallel numerical simulations.

Dr. Murphy was a recipient of a Hamilton Scholarship from the Dublin Institute for Advanced Studies in 2004.



Mark E. Dieckmann received the M.Sc. degree from the University of Sussex, Brighton, U.K., in 1995 and the Ph.D. degree in computational plasma physics from the University of Warwick, Coventry, U.K., in 1999.

He is currently an Associate Professor with Linköping University, Linköping, Sweden. He was a Visiting Professor with Queen's University Belfast, Belfast, U.K., in 2008–2009. His research interests include numerical particle-in-cell simulations of the dynamics of plasmas far from their thermal equilibrium and the visualization and interpretation of the simulation data, more specifically in the areas of energetic astrophysical plasma flows (e.g., jets and shocks), and modeling of the interactions between laser pulses and plasma.

librium and the visualization and interpretation of the simulation data, more specifically in the areas of energetic astrophysical plasma flows (e.g., jets and shocks), and modeling of the interactions between laser pulses and plasma.



L. O'C. Drury received the B.A. degree in pure mathematics and experimental physics from Trinity College Dublin, Dublin, Ireland, in 1975 and the Ph.D. degree from the University of Cambridge, Cambridge, U.K., in 1979. His Ph.D. thesis focused on fluid dynamical problems in astrophysics.

He is a theoretical astrophysicist with a strong interest in computational methods. After receiving the Ph.D. degree, he joined the Max-Planck Institut fuer Kernphysik, Heidelberg, Germany, where he was promoted to a Senior Research Associate. He

is currently a Senior Professor with the School of Cosmic Physics, Dublin Institute for Advanced Studies, Dublin. His current research interests are particle acceleration in shock waves and the origin of cosmic rays.

Prof. Drury was a recipient of a gold medal in physics from Trinity College Dublin.